Investigations on Stability of Cylindrical Shells under Axial Compression

R.Palaninathan[1)], K.Athiannan[2)], G.Thomas[1)].

1) Solid Mechanics Division, Department of Applied Mechanics, Indian Institute of Technology, Madras, India.
2) Reactor Group, Indira Gandhi Centre for Atomic Research, Kalpakkam, Tamil Nadu, India.

ABSTRACT

This paper deals with the experimental studies on circular cylindrical shell models under axial load and the correlation of the same with the analytical values obtained from the finite element (FE) models. The geometric details of the models are: H/R ≈ 1 and R/t = 437.5, 350.0 and 280.0 for the thicknesses of t = 0.8, 1.0 and 1.25 mm respectively. The models are fabricated using stainless steel grades 304 and 316 by rolling and TIG welding. The experimental setup consists of: rectangular frame, hydraulic loading system with air intensifier for maintaining the load constant during buckling, LVDTs for initial geometric imperfection measurements, strain gauge in pairs (inside and outside), three load cells, 120° apart to ensure uniform distribution of axial load and a data logger. The load is applied in steps till failure of the specimen. The deformed configurations and strains are plotted as functions of load. Deformation in general follows the initial geometric imperfection shapes. The amplitude of the imperfections are found to vary from specimen to specimen, a minimum of 1.2 t to a maximum of 5.75 t. Initially, strains vary linearly with load and undergo sudden changes in the vicinity of failure load. This helps to pinpoint the buckling load graphically. The imperfections are imposed both in axial and circumferential directions as obtained from the experimental models. In this respect, the present study differs from most of the earlier works, wherein the imperfection shapes are matched with the critical buckling modes with the specified amplitude-to-thickness ratios. The analytical limit loads with and without imperfections are obtained using ABAQUS FE software, treating the problem as a general non-linear one. The correlation of the experimental and analytical values is made. The average experimental value is lower than the analytical value with real imperfection imposed.

INTRODUCTION

For thin walled structures, the stability criterion controls the design, as the structure fails at very low stress level due to loss of stability much lower than the yield stress. If the shell is loaded such that most of its strain energy is in the form of membrane compression and if this stored-up membrane energy can be converted into bending energy, the shell may fail rather dramatically in a process called buckling, as it exchanges its membrane energy for bending energy. Very large deflections are generally required to convert a given amount of membrane energy into bending energy. In other words, the structure goes from one equilibrium position (pre-buckling state) to another (buckled state); i.e., it has multiple equilibrium configurations. The classical buckling equations are derived based on the above concept. The above idealised conditions are not seen to exist in real structures and hence the values obtained from the classical equations are very high. This situation has prompted the structural analyst to study extensively the buckling problems both experimentally and analytically.

In a pool type Liquid Metal Fast Breeder Reactor (LMFBR) design, the main vessel is one of the important components. The design of such structures is controlled by the seismic loading during which the vessel is subjected to horizontal shear and bending. The radius- to- thickness ratio (R/t) of this vessel is very large and is prone to fail by buckling. The buckling behavior of cylindrical shells due to bending may be equivalent to that under axial compression. Since the main vessel is classified as class 1 component, according to ASME Boiler and Pressure Vessel code, section III, subsection NB [1], the structural integrity is to be checked experimentally to validate the design. Keeping this in mind, a test programme has been formulated at Indira Gandhi Centre for Atomic Research (IGCAR) to carry out experimental studies on scale models under axial and shear loads. This paper presents the first stage of study on axially compressed cylindrical models.

BRIEF HISTORICAL NOTES

The studies on shell buckling started about 150 years ago by Fairban in England and the motivation was the design of tubular bridges, a civil engineering application. The developments in boiler design for mechanical and marine applications kindled further interest on shell buckling studies. Subsequently, the advances in aerospace and nuclear fields increased the awareness and the need for experimental studies on unstiffened and stiffened shells. Considerable amount of literature exists on buckling studies carried out by the earlier researchers. The historical developments on this field may be obtained from the three recent review papers [2], [3], [4].

Cylindrical shells under axial compression have been investigated by both analytical and experimental methods quite extensively. The comparisons between the two have revealed wide differences. Also, there has been large scatter between the experimental values. The reasons for this discrepancy have been traced to: the effect of initial geometry imperfection;

eccentricity between the loading and the specimen axes; influence of boundary conditions. The scatter in the experimental values has been attributed to the differences in the magnitude and the shape of the initial imperfections between the specimens, even though they are fabricated by the same method. Considerable amount of attention has been paid on the study of the effect of initial geometric imperfections. The cylindrical shells under axial compression are found to be highly sensitive. It was Koiter who gave theoretical explanation for the influence of imperfection on the buckling loads. He dealt directly with the imperfect configuration by perturbing the perfect geometry using the imperfections of small magnitude in the form of critical buckling mode [5]. With the presence of initial imperfection, the character of buckling analysis changes from classical eigen value to nonlinear problem. The analyst has to follow the load-deflection path and predict the failure either at limit point or at the bifurcation point. In the analytical modeling of imperfect geometries the method of eigen mode injection has been adopted by many authors [6]. This is a two stage process in which first, the critical eigen mode is obtained and then this eigen mode is perturbed / normalised with respect to the maximum initial geometric imperfection of assumed magnitude or experimentally observed maximum. Very few studies have been reported on modeling the structure using real imperfection [7].

In the present study the objectives are two fold: one, to make a comparative study of the failure loads of the experimental and the analytical models; two, to generate imperfection data on fabricated shell models.

EXPERIMENTAL WORK

Specimens

Scale models of radius, R = 350mm (approximately $1/18^{th}$), effective height, H = 340 mm (overall height, L = 450 mm) and three thicknesses (t = 0.8, 1.0 and 1.25 mm) are fabricated. Totally 12 models are tested. They are divided into three groups of four each. Table 1 gives the geometric details of the 12 models. These are fabricated by rolling and TIG welding. Models of 0.8 and 1.0 mm thicknesses are made using stainless steel grade 316 and for 1.25mm thickness, stainless steel grade 304 is used. Stress reliving is not done for all the models, as the residual stresses arising from the welding are expected to be very small. Fig. 1 shows the details of the models. Thick flanges machined to 0.01 mm accuracy are fitted on the models by bolts at the ends. This ensures circularity. Verticality of the shell wall and the parallelism of the flanges are also checked on surface plate. The material properties required for analytical modeling are obtained through systematic tensile testing on coupons taken from the corresponding sheet metal.

Table 1. Geometric Details of Models

Group	Model #	t	R	R/t	H	L	H/R
I	1	0.80	350	437.5	340	450	≈1
	2	0.80	350	437.5	340	450	≈1
	3	0.80	350	437.5	340	450	≈1
	4	0.80	350	437.5	340	450	≈1
II	5	1.00	350	350.0	340	450	≈1
	6	1.00	350	350.0	340	450	≈1
	7	1.00	350	350.0	340	450	≈1
	8	1.00	350	350.0	340	450	≈1
III	9	1.25	350	280.0	340	450	≈1
	10	1.25	350	280.0	340	450	≈1
	11	1.25	350	280.0	340	450	≈1
	12	1.25	350	280.0	340	450	≈1

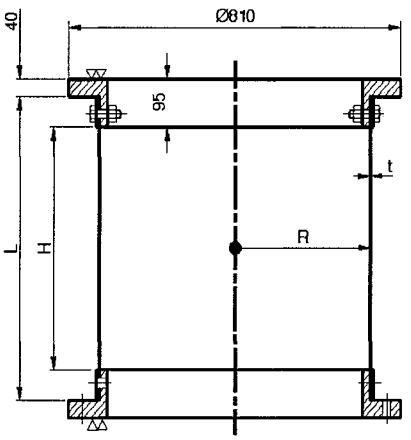

Fig.1 Models with End Fittings

Experimental Setup

An experimental test facility has been designed, fabricated and installed for the present work, Fig. 2. In this facility, both axial and shear buckling tests can be carried out. Maximum capacity of the test rig is 100 t for axial and 15 t for shear loads. A double acting hydraulic jack (1) is fixed at the middle of the cross beam. A power pack (11) with air intensifier system is used to operate the hydraulic jack. The advantages of using air intensifier system are: a) it helps in smooth application of load, b) maintain load constant at specified level, c) quick response during buckling. Three load cells (2) are kept at 120° apart on the bed (3). A conical loading frame (8) with flanges on both ends machined to the accuracy of 0.01 mm and checked for parallelism is placed on the top flange of the specimen and bolted. A guide plate is placed on the top of the conical frame with sliding fit. When the hydraulic jack is actuated, the ram moves through the central hole on the guide and rests on the top of the conical frame. Thus the alignment of the loading system is ensured.

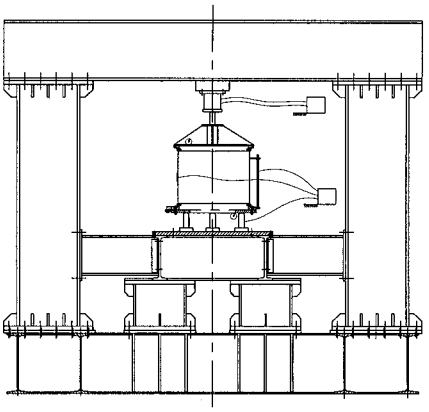

Fig. 2a Experimental Set up for Axial Load

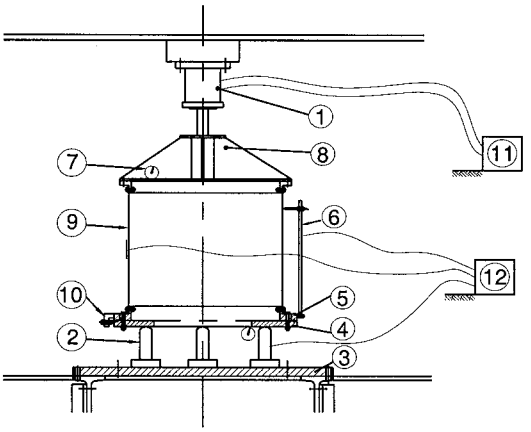

Fig. 2b Enlarged View of the Shell Assembly

Imperfection survey is carried out using Linear Variable Differential Transformers (LVDTs), which are mounted on a special arrangement. This consists of a machined annular plate (4) coaxially bolted with the bottom flange of the specimen with overhang. On the overhang portion of the annular plate, 8 spherical balls are kept in the grooves, which are equidistant apart. A ring (5) is placed around the bottom flange of the specimen with sliding tolerance and is resting on these balls. This enables free rotation of the ring about the specimen axis. Four LVDT holders (6) of different heights are fixed on the ring at 40°, 90°, 180° and 270°. On these holders LVDTs are mounted normal to the specimen surface. The holder at 40° location can move upto a distance of 95 mm from bottom. Similarly, others can move in the three-quarters of the specimen height. A spring loaded indexing mechanism is fixed at 0° in the ring (5). The annular plate (4) has been graduated on the periphery, enabling imperfection measurements at every 5° intervals or its multiples. Three pairs of dial gauges placed at 120° apart are used to measure the end shortening. In a pair, one is kept on the top and the other is kept on the bottom. Four pairs of strain gauges are pasted at half the height of the cylinder, 90° apart. In a pair, one is pasted on inner and the other pasted on the outer surface at the same location. Load cells, LVDTs and strain gauges are connected to the Data Acquisition System of M/s Measurement Group, USA.

Test Procedure

Imperfection Survey

After mounting the specimen on the test bed as described above, the imperfection survey is first carried out. LVDT readings are taken at 5° intervals at 4 levels, 95mm, 170mm, 245mm and 320mm, from the bottom support. After each sweep, the LVDTs are lowered by 15mm and the scan is continued. The shifting is done 4 times. In other words, readings are taken at 20 equidistant levels along the length of the specimen, which works out to 1440 points (72X20). The raw data obtained from the LVDTs are processed to obtain the initial geometric imperfection, δ_i, the eccentricity, e, using the following equation,

$$\delta_i = \Delta r_i + \Delta r' - a\sin\theta_i - b\cos\theta_i \qquad (1)$$

where Δr_i is the LVDT reading location, i, $\Delta r' = -\dfrac{\Sigma \Delta r_i}{n}$,

$$a = \frac{2}{n}\Sigma \Delta r_i \sin\theta_i, \qquad b = \frac{2}{n}\Sigma\, \Delta r_i \cos\theta_i,$$

n is the number of LVDT readings around the circumference, Eccentricity, $e = \sqrt{a^2 + b^2}$.

Loading

Subsequent to the imperfection survey, the loads are applied in steps. The numbers of steps are varied from specimen to specimen with minimum 9 and maximum 13. At all load steps, the load cells, strain gauge and dial gauge readings are recorded. At selected load steps, LVDTs scans are carried out. LVDTs are removed at about 70% of the analytically computed value. Subsequently, finer increments in loads are applied till the specimen fails.

ANALYTICAL WORK

Finite element based general purpose computer program, ABAQUS [8] is used for estimating the failure load of the specimen. The modeling is done using 4-noded quadrilateral shell element (S4R5). The general nonlinear option (both material and geometric nonlinearlity) is employed. Failure loads are obtained under three cases.

i) perfect geometry
ii) eigen mode injected imperfect geometry
iii) geometry with real imperfection

Perfect Geometry

Firstly, eigen value analysis is carried out to provide guidance in mesh design, because mesh convergence studies are needed to ensure the minimum eigen value estimate. A half wave circumferentially subtends an angle, $\alpha = \pi/n$, where n is the number of circumferential waves. The region considered for Finite Element (FE) modeling consists of half the length in the axial direction and an arc length equal to one half wave in the circumferential direction. 30 divisions in the circumferential direction and 40 divisions in the axial direction are used. Symmetry boundary conditions are imposed on both the longitudinal edges and at the bottom (middle half). At the top, all the degrees of freedom (dofs) are arrested except the displacement in the axial direction. Parametric studies are made for all thicknesses by varying n from 3 to 12 to estimate the lowest critical load. From these studies, $\alpha = \pi/11$, $\pi/10$ and $\pi/9$ are the angles obtained for the thicknesses, t = 0.8, 1.0 and 1.2 mm respectively. Fig. 3 shows the FE mesh of perfect geometry.

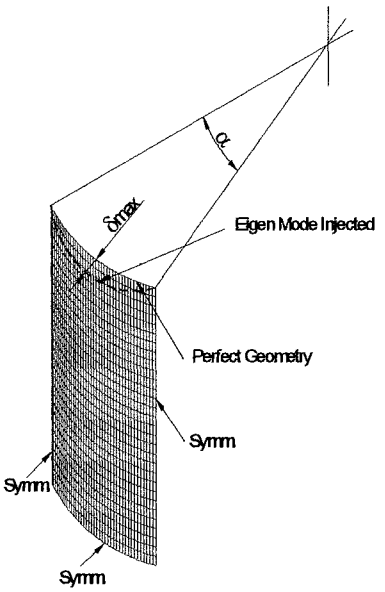

Fig 3 FE Mesh for the Perfect and Eigen Mode Injected Geometry

Eigen Mode Injected Imperfect Geometry

The measured maximum imperfection value $\delta_{max.}$ is added to the radial coordinate of the node of the perfect geometry, Fig. 3. The eigen mode is re-normalised with respect to $\delta_{max.}$. FE mesh, boundary conditions and loading are same as of the previous case.

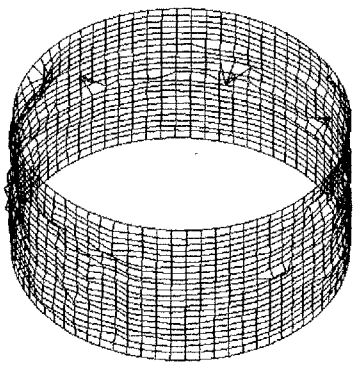

Fig 4 Finite Element Idealization, Model # 11 (Magnification factor =15)

Geometry with Real Imperfection

The imperfection introduced by the above method does not represent the actual imperfection existing in the specimens. The imperfections found in the fabricated models have arbitrary variations both in the circumferential and the axial directions, which calls for the consideration of full cylinder in FE idealisation. For handling this type, the imperfection shape is decomposed the into several Fourier modes, the dominant modes are identified and analysis is carried out for these modes. The imposition of imperfection necessarily calls for the use of nonlinear analysis option and hence the above superposition method is not considered valid. A better representation is the incorporation of the measured imperfection in FE mesh directly. The nodes of the FE mesh are made to coincide with the imperfection measuring points (1440 locations). A computer program is written to add the measured imperfection values to the radial coordinates of the corresponding nodes in the FE mesh. The nodes on the boundary are not imposed with any imperfection. 72 divisions in the circumferential and 22 divisions in the axial directions give 1656 nodes and 1584 elements in the FE model. The FE idealisation is shown in Fig. 4. The imperfection values have been magnified 15 times in Fig. 4 for the shake of clarity. All the dofs at the bottom are arrested. At the top, as the load is applied, the displacement in the axial direction is allowed and other dofs are arrested.

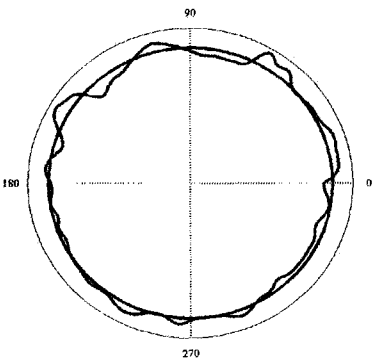

Fig. 5 Initial Geometric Imperfection, Model # 6, Height = 245 mm from bottom (Magnification factor = 40, $\delta_{max.}$ = 0.8 mm)

RESULTS AND DISCUSSIONS

Initial Geometric Imperfections

In all 12 tests, as given in Table 1, the relevant data are recorded for further analysis. Initially, imperfection survey is carried out as explained already under the test procedure. The raw data are processed using the equation (1) for the imperfection

values. The imperfection shape at 245 mm from the bottom of the shell for the model #6 is shown in Fig. 5. Fig. 6 shows the three-dimensional mapping of the initial geometric imperfection of the model # 11. Table 2 gives the imperfection data of all the 12 models along the axial direction at a circumferential location, θ where the maximum imperfection occurs. The circumferential angle θ is measured from a reference point on the annular plate (4). Among all the specimens, model # 12 is found to have largest outward imperfection of 4.726 mm, which is equal to 3.78 t. In the case of model # 4, the maximum imperfection (outward) is 4.6 mm, which is equal to 5.75 t. The locations of the weld line are also given in the Table 2. It is seen that the locations of $\delta_{max.}$ do not coincide with the weld lines in any of the models. It is observed from the imperfection data of all the twelve models that the scattering and the maximum imperfection (multiples of thickness) decreases as the thickness increases.

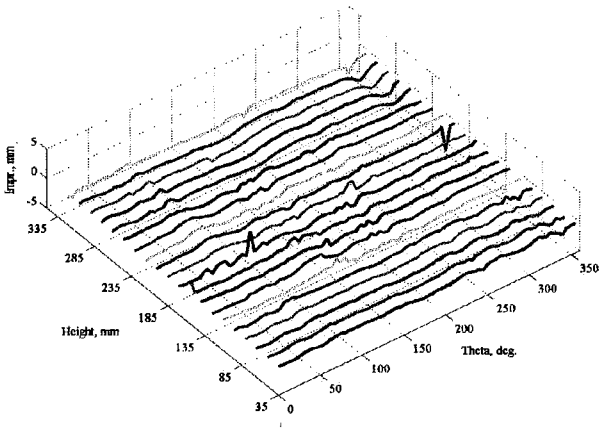

Fig. 6 3-D Mapping of Initial Geometric Imperfection, Model # 11, $\delta_{max.}$ = 3.7 mm

Table 2. Initial Geometric Imperfections (mm), $\delta_{max.}$ along the axial directions

Model #											
1	2	3	4	5	6	7	8	9	10	11	12
Circumferential location, θ											
200	120	220	300	40	15	275	5	105	185	345	345
Weld line, θ											
70	220	195	340	95	135	355	85	135	10	245	315
Imperfection, mm											
0.457	-0.053	0.098	0.085	0.089	0.512	0.933	0.147	0.487	-0.195	-0.118	0.444
-0.065	-0.15	0.117	0.049	-0.273	0.422	0.578	-0.192	0.601	-0.240	-0.049	0.568
-0.127	-0.151	0.078	0.142	-0.237	0.496	0.593	-0.261	0.562	-0.291	-0.076	0.287
-0.066	-0.213	0.103	0.108	-0.462	0.415	0.796	-0.094	0.537	-0.182	-0.195	0.173
-0.116	-0.056	0.073	0.196	-0.256	0.521	2.882	-0.404	0.445	-0.142	-0.072	0.301
-0.360	-0.277	-0.079	0.157	-0.132	0.139	1.569	-0.769	-0.214	0.396	-0.006	-0.375
-0.028	-0.261	0.020	0.328	-0.183	-0.023	-0.168	-0.830	-0.278	0.411	0.301	-0.439
3.016	-0.290	2.208	0.221	-0.075	-0.333	0.000	-0.681	-0.299	0.733	-0.057	4.726
-0.366	-0.321	-0.39	-0.104	-0.2	-0.214	1.239	-1.040	3.039	0.628	0.043	-0.072
0.154	-0.344	-0.134	4.606	3.312	-0.211	1.189	-0.761	-0.405	0.156	-0.060	-0.513
-0.568	-0.296	0.143	-0.133	-0.35	0.944	0.498	-1.520	0.299	-0.120	-0.096	-0.513
0.189	-0.591	0.153	-0.105	-0.38	0.429	-0.199	-1.559	0.026	-0.063	-3.735	0.160
0.244	-0.786	0.175	-0.071	-0.446	0.095	-0.326	-1.569	0.037	-0.082	0.022	0.275
-0.411	-1.034	0.225	-0.016	-0.166	0.806	0.567	-1.694	0.113	-0.067	-0.168	0.070
0.201	-1.022	0.204	-0.320	-0.387	2.014	0.523	-1.867	0.126	-0.192	-0.386	-0.135
0.207	-0.048	0.084	-0.133	0.127	-0.836	-0.479	1.299	-0.171	-0.348	-0.597	0.443
0.093	-0.068	0.153	-0.234	0.114	-1.198	-0.429	1.247	-0.881	-0.496	-1.453	0.495
0.135	-0.043	0.220	0.109	-0.007	-0.022	-0.391	1.080	-1.018	0.083	-0.649	0.284
0.074	-0.012	0.132	-0.679	0.091	-0.194	0.142	0.991	-0.172	-1.321	-0.478	0.620
0.148	0.072	-0.112	-0.313	-0.075	-0.120	-0.052	0.821	-0.030	0.495	-0.121	0.490

Failure Load

Initially load is applied in increments of 20 kN. Subsequently it is reduced to 10 kN and further reduced to finer increments till the failure occurs. The air intensifier helps to apply the load in finer increments smoothly during later stages. LVDT scans are carried out at few load steps to observe the growth of radial deformation during loading. In general, it is found that the growth of radial deformation resembles that of initial imperfection shape. The failure is observed through the formation of lobes in the central region of the shells. The lobe formation starts at one location and spreads subsequently in the circumferential direction followed by a big thud. It is noted that for 0.8 mm thickness, the formation of lobes start at the weld line for all the four models. This is due to softening of the material at the weld zone. The heat input could not be reduced further to match the requirement of thinner sheet due to the limitation of the welding equipment. The photograph of one of the buckled models is shown in Fig. 7. It is seen that the lobes are formed in the middle region and the total number of lobes is 13. Table 3 gives the comparison of experimental and analytical failure loads of all the 12 models. In the case of models, 1-4 (group I) the average experimental failure load is 145 kN and difference between the lowest and the highest is 27.2 kN (18.8% scatter). A comparison between the experiment and the analytical results of this group reveals the following. Geometry with real imperfection predicts higher failure load (average load = 202 kN) than the experimental one (39.3% difference). The model with eigen mode injected imperfect geometry gives the average failure load of 138.6 kN (-4.4% difference) which is closer to the experimental value. The lower value in the case of the latter is due to the fact that **excessive imperfection** has been imposed. In other words, the maximum imperfection found in one place in the experimental model is set at 2n points, where n is the number of circumferential waves. The failure load of the perfect geometry model is 367.4 kN and is same for all the models in the group. This value is more than twice the experimental value. In the case of models, 5-8 (Group II), the results are summarised as follows. The average experimental failure load is 235.3 kN with difference between the lowest and the highest is 27.6 kN (11.7% scatter). Geometry with real imperfection gives average value of 295.5 kN (25.6%difference) whereas eigen mode injected imperfect geometry gives the average value of 195.7 kN (-16.8% difference). The failure load of the perfect geometry model is 524 kN. In the case of models 9-12 (Group III) the results are: the average experimental failure load is 309.4 kN and difference between the lowest and highest is 34.3 kN (11.1% scatter). Geometry with real imperfection gives

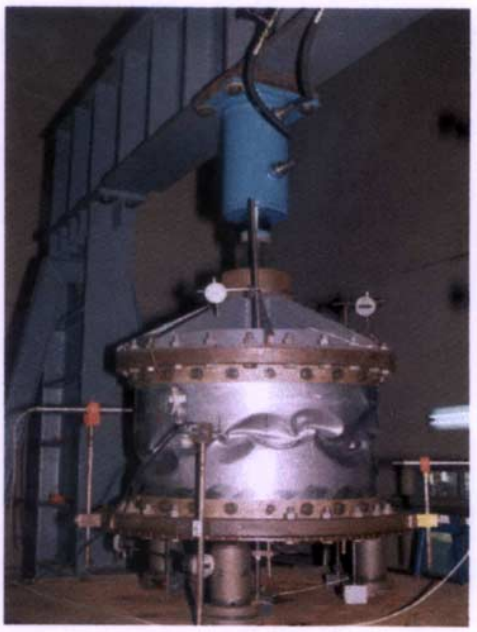

Fig 7 Buckled Shell, Model # 6

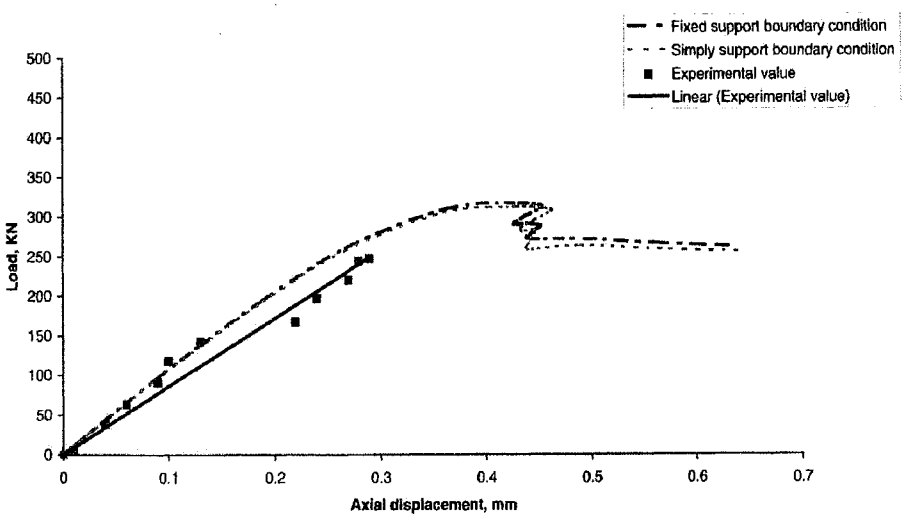

Fig 8 Load vs Axial displacement, Model # 8

average value 489.4 kN (55% difference). Eigen mode injected imperfect geometry gives the average value 287.6 kN (-7% difference). The failure load of the perfect geometry model is 592.9 kN. From the results, it is observed that the scatter in the experimental failure loads decreases as the thickness increases. It is seen that the FE model with real imperfection predicts higher load in all the three groups. The reasons for this difference may be attributed to the eccentricity between the loading and the specimen axes. Since as observed in the earlier section, there are three reasons for the difference between the analytical and experimental values. They are: the effect of initial geometry imperfections, eccentricity between the loading and the specimen axes and the influence of boundary conditions. FE modeling with real imperfection includes only the initial geometric imperfections. Also, in the finite element modeling, the boundary condition imposed is clamped one whereas the boundary conditions realised in the experimental model differ from this. When the boundary condition is of FE model changed to simply supported condition, there is no appreciable difference in the analytical value. Average value of the end shortening obtained from the 3 pairs of dial gauges is plotted against load, Fig. 8. This leads to the conclusion that the eccentricity between the loading and the specimen axes is mainly responsible for the difference between the experimental and analytical values with real imperfection. From literature, it is seen that no researcher has paid attention to quantify this effect. Residual stresses introduced by the fabrication process may also be a contributing factor to this discrepancy. However, it is possible to isolate this effect by stress relieving of the specimens. It is observed from Table 3, failure load for the eigen mode injected imperfect geometry are not varying according to the magnitude of the imperfection present in the specimens. This is due to fact that the specimen undergoes elasto-plastic deformation during buckling. Presence of imperfections in the plastic region does not have any influence on the limit load. It is affected by the presence of imperfections mostly in the elastic region. Fig. 9 shows the Von Mises stress contour of the model #1 for the eigen mode injected imperfect geometry. The stress level in some portion of the segment exceeds the yield strength. The variations of axial strain with load of the 4 pairs of strain gauges for the model # 6 are shown in Fig. 10. Initially the strains are increasing linearly with load. During buckling the response of all the gauges show sudden changes. In a pair, the two gauges show opposite signs. This helps to pinpoint the failure load of the specimen.

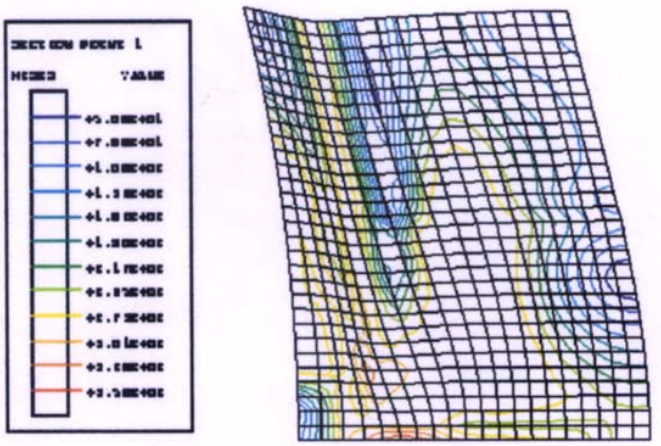

Fig 9 Stress Contour, Model # 1
(Eigen Mode Injection Method)

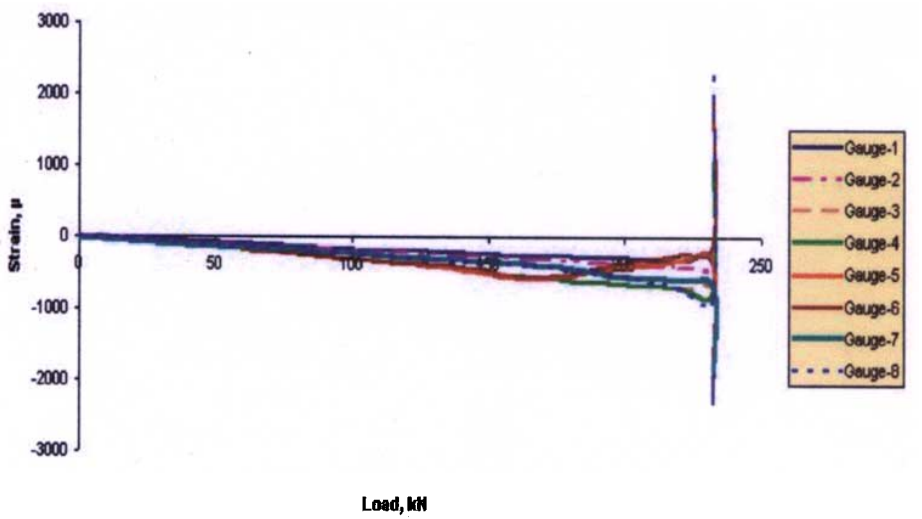

Fig 10 Axial Strain vs Load, Model # 6

Table 3. Comparison of experimental and analytical failure loads of the models

Group #	Model #	Thickness t (mm)	Max.Imp. (mm)	Limit Load, kN			
				Exp.	Real Imp.	Eigen mode injection	Perfect Geometry
I	1	0.8	3.03	163.1	157.5	137.5	367.4
	2		1.03	135.9	229.0	149.6	
	3		2.2	140.6	210.0	138.6	
	4		4.6	140.0	210.8	128.7	
II	5	1.0	3.3	242.2	270.0	220.0	524.0
	6		2.01	232.5	310.0	180.0	
	7		2.88	219.5	285.0	200.0	
	8		1.86	247.1	317.0	182.7	
III	9	1.25	3.03	320.1	474.0	239.4	592.9
	10		1.32	321.0	559.3	396.0	
	11		3.7	309.8	540.6	244.8	
	12		4.7	286.7	383.8	270.0	

SUMMARY

The objective of this work is to estimate the initial geometry imperfection in the fabricated models and also to make correlation between the experimental and the analytical failure loads. Among the 12 models tested, the maximum imperfection is 5.75 t (outward) and minimum 1.2 t (inward). The magnitude of imperfection is expressed, as multiples of thickness with imperfection is higher in the thinner models. The complete initial imperfection data for all the 12 models in the form of three-dimensional mapping have been generated. As for the correlation of the experimental and the analytical failure loads, the experimental values are bracketed between that of two analytical models, one with the real imperfection and the other with the eigen mode injected imperfection. The real imperfection models always predict higher loads because the other equally influencing factor, namely, the eccentricity between the loading and the specimen axes is not accounted for. The experimental values are closer to the eigen mode injected model. This is the observation one can note from all the three groups of the models, i.e., the failure load obtained from the eigen mode injected FE model gives always the lower bound values. It is difficult to draw the conclusions whether to use this model for the design of prototype structures as data on hand is limited.

ACKNOWLEDGEMENT

The authors gratefully acknowledge the excellent support and encouragement provided by Shri. S.B. Bhoje, Director, Shri. S.C. Chetal, Associate Director, Design and Technology Group and Dr. P. Chellapandi, Head, Mechanics and Hydraulics Division.

REFERENCES

1. ASME Boiler and Pressure Vessel Code, 1995.
2. Bushnell, D., "Buckling of Shells – Pitfall for Designers," AIAAJ, Vol. 19, No. 9, 1981, pp 1183-1226.
3. Singer, J., "Experimental Studies in Shell Buckling," Proc. Of the Structural Dynamics and Material Conference, AIAA, Newyork, USA, Vol. 3, 1997, pp 1922-1932.
4. Teng, J.G., "Buckling of Thin Shells: Recent Advances and Trends," ASME, Applied Mechanics Review, Vol.49, No. 4, 1996, pp 263-274.
5. Hutchinson, J.W., and Koiter, W.T., "Post Buckling Theory," ASME, Applied Mechanics Review, Vol.23, 1970, pp 1353-1366.
6. Matsuura, S. et. al., "Buckling Strength Evaluation of FBR Main Vessel under Lateral Seismic Loads," Transactions of the 11th International Conference on Structural Mechanics in Reactor Technology, Vol. E, Tokyo, Japan, 1991, pp 269-280.
7. Schneider. Jr, M.H., "Investigations of the Stability of Imperfect Cylinders using Structural Models," Engineering Structures, Vol. 18, No. 10, 1996, pp 792-800.
8. ABAQUS USER'S MANUALS, Version-5.5, Hibbitt, Karlsson & Sorensen, Inc. 1080 Main Street, Pawtucket, RI 02860 - 487, USA.